Inorganica Chimica Acta 507 (2020) 119584

Contents lists available at ScienceDirect

Inorganica Chimica Acta

journal homepage: www.elsevier.com/locate/ica

Research paper

Surface molecular engineering of axial-exchanged Fe(III)Cl- and Mn(III)Cl-porphyrins towards enhanced electrocatalytic ORRs and OERs

Isaac Kwaku Attatsi[a,b], Weihua Zhu[a,b,*], Xu Liang[a,*]

[a] School of Chemistry and Chemical Engineering, Jiangsu University, Zhenjiang 212013, PR China
[b] School of Environment and Safety Engineering, Jiangsu University, Zhenjiang 212013, PR China

ARTICLE INFO

Keywords:
Noncovalent immobilization
Metalloporphyrin
Electrocatalysis
Oxygen reduction
Oxygen evolution

ABSTRACT

Herein, pyrene-pyridine (Pyr-Py) molecule was applied as the axial exchanged ligand to bridge Fe(III) and Mn (III)porphyrin immobilized on rGO. These axially exchanged metalloporphyrin functionalized nanocomposites revealed enhanced electrochemically catalyzed oxygen reductions and evolutions that demonstrated the surface molecular engineering through axial ligand exchange is an effective strategy to enhance the catalytic efficiency.

1. Introduction

The upsurge in global warming owing to increasing demand and usage of fossil fuels has being a matter of concern to environmental engineers [1,2]. This has necessitated a search for clean, cheap, and highly efficient energy systems which serve as alternative to fossil fuels [3,4]. Electrochemical oxygen reduction reactions (ORR) and oxygen evolution reactions (OER) play important role in many energy conversion systems, such as fuel cells, metal-air batteries [5–7] and electrocatalysis [8,9]. The major challenge associated with these reactions is their sluggish kinetics at cathodes of fuel cells [10,11]. Owing to this challenge, molecular electrocatalysts with advances in research are developing new ways to eliminate the sluggish kinetics of ORR in other to make fuel cell technology well appreciated [12]. Traditionally, noble metal Pt is used in energy conversion devices as a form of replacement to fossil fuels but due to high cost [9,13], instability, scarcity [14] and ease of methanol poisoning arising from Pt, its use could not be sustained [15,16]. After series of research, molecular catalysts from earth-abundant 3*d* transition metals such as Mn [17,18] and (Co/Fe) [19–21] showed to be a better alternative to Pt based catalyst, such as metalloporphyrin [22–24]. Recently, Wang and co-workers reported on metal porphyrin intercalated rGO nanocomposite as efficient electrocatalyst for oxygen reduction [25]. Previously, Zuo reported the orientation mode of Co(II)porphyrins for electrocatalytic dioxygen reduction [26], and Marianov's group discussed the covalent and/or noncovalent immobilized Mn(III)Cl-TPP towards electrocatalytic water oxidation and oxygen reductions [27]. On the other hand, Wei and Chlistunoff focused on the bio-inspired axial ligand coordinated iron (III) porphyrin in an ordered manner for enhanced oxygen reduction [14,28]. Thus, surface molecular engineering of axial-exchanged metalloporphyrinoids became one of the interesting topics towards enhanced ORR activity and stability compared to both non-axially linked metalloporphyrin and Pt/C catalyst in aqueous media especially. Insight from these studies reveals the enhanced electrocatalytic performance of metalloporphyrins especially when axially coordinated. It should be pointed here, when pyrene-pyridine hybrid (**Pyr-Py**) was used as the key linker, both axial exchanged behaviors and surface order assembling could be facilely included within one system. Thus, the current investigations will provide useful information on how functionalized linkers work for surface molecular engineering towards enhanced catalytic behaviors (Scheme 1).

2. Results and discussions

2.1. Spectroscopic investigations

Mn(III)Cl-tetraphenylporphyrin [27] **2** and pyrene-pyridine [29] (**Pyr-Py**) were prepared according to literature procedures (Scheme S1, see ESI), and Fe(III)Cl-tetraphenylporphyrin was commercially purchased. Upon introduction of 0.4 μM **Pyr-Py** solution to **1** and **2**, **Pyr-Py** characterization peaks surfaced in addition to a decrease in both Soret and Q absorption bands of **1** and **2** (Fig. 1**a** and **b**) [30,31]. When pure pyridine was added, new bands related to metalloporphyrins appeared [28], a behaviour which wasn't seen using **Pyr-Py** (Fig. 1**c** and **d**). Despite this occurrence, decrease in absorption bands of metalloporphyrins appeared during introduction of either pyridine or Pyr-Py. It is

* Corresponding authors at: School of Chemistry and Chemical Engineering, Jiangsu University, Zhenjiang 212013, PR China.
E-mail addresses: sayman@ujs.edu.cn (W. Zhu), liangxu@ujs.edu.cn (X. Liang).

https://doi.org/10.1016/j.ica.2020.119584
Received 22 December 2019; Received in revised form 5 March 2020; Accepted 5 March 2020
Available online 13 March 2020
0020-1693/

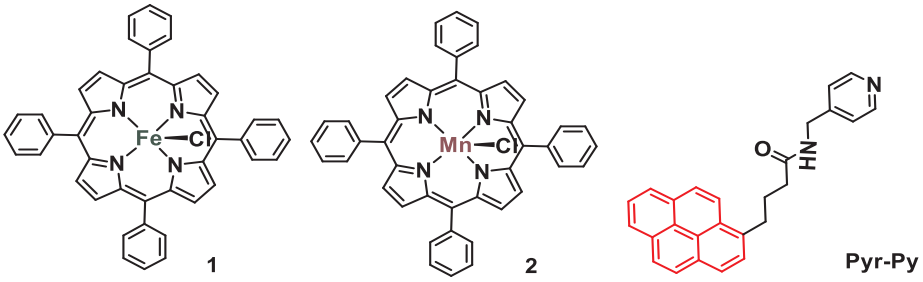

Scheme 1. Molecular structures of Fe(III)Cl-TPP (left), Mn(III)Cl-TPP (middle) and **Pyr-Py** (right).

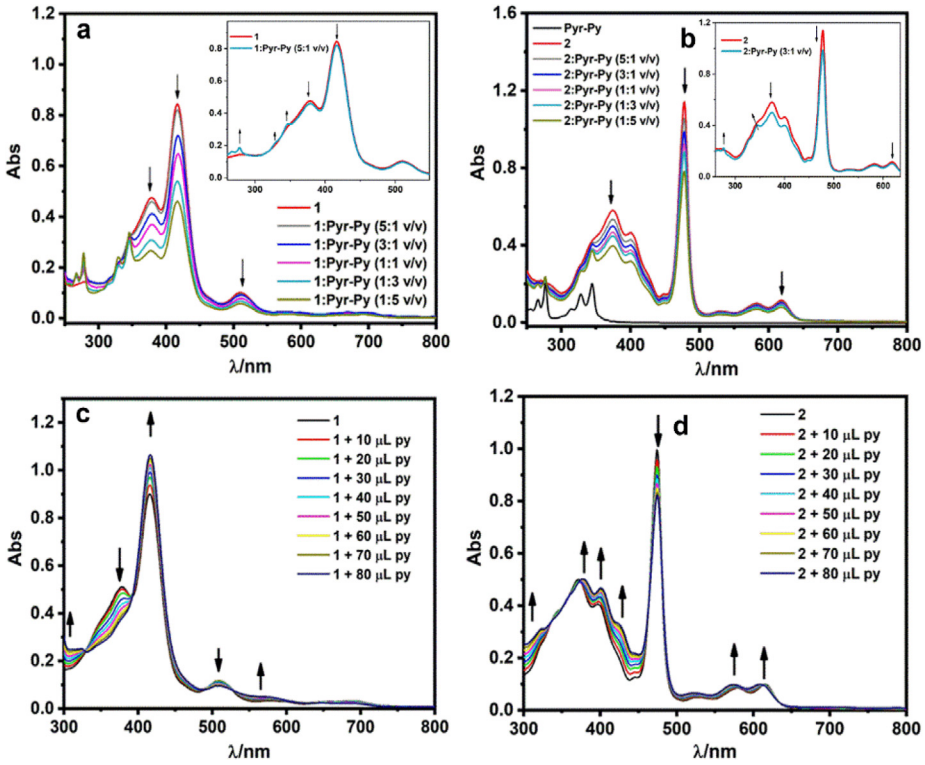

Fig. 1. UV–vis spectra of **1** and **2** upon addition of 0.4 μM **Pyr-Py** (**a** and **b**) and 12.35 M pure pyridine (**c** and **d**) in CH_2Cl_2.

worthy to note that as equivalent ratios of **Pyr-Py** increases its absorption spectra begin to appear clearly. This is consistent with the work of snitkoff et al., where the imidazole peaks increase as the ratio of the linker increases [31]. On the other hand, axial exchange could also be confirmed when UV–vis spectra of rGO composite materials are measured. As shown in Fig. S1, the appearance of **1** and **2** together with our **Pyr-Py** in our composite materials showed little or no change in both Soret and Q-band wavelength but a minimal decrease in absorption intensity which is consistent with results obtained in solution devoid of rGO. This observation could arise from coordination interaction. Another observation is the rise in baseline of the composite materials which is attributed to the presence of rGO in the nanocomposites. At the same measuring conditions, spectroscopic evidence to support direct interaction between metalloporphyrin **1** and **2** to rGO is the appearance of respective metalloporphyrin peaks at both the Soret and Q regions accompanied with a rise in absorption bassline (Fig. S1, see ESI).

2.2. Structural characterizations

Morphological characterization of rGO and its supported nanocomposites using SEM showed the good exfoliated structure (Fig. 2), besides, no significant aggregation or decomposition were observed upon introducing metalloporphyrin **1** and **2** [32,33] as well as **Pyr-Py**. Also, XRD patterns of rGO, **1**/rGO and **1**/rGO/**Pyr-Py** showed broad peaks around 25° which is a characteristic feature of rGO as shown in Fig. 3**a** and **c**. This diffraction angle is indexed to graphitic sheet of reduced GO related to [0 0 2] diffraction of graphene sheet [34], besides XRD measurement didn't show any assigned metallic peaks. In addition, these rGO supported nanocomposites were also characterized by FT-IR spectroscopy (Fig. 3**b** and **d**). Composite materials of **1** showed the characteristic peaks of tetraphenylporphyrin itself, for example, a broad band at ca. 3052 cm^{-1} is assigned as the C—H bond stretching in phenyl rings of **1**. Peaks at 1594 cm^{-1} (C═C stretching vibrations of phenyl rings), 1444 cm^{-1} (C═C), 1337 cm^{-1} (C—N), 1071 cm^{-1} (C═C stretching vibrations of pyrrole ring), 1001 cm^{-1} (C—C vibrations of pyrrole ring), 808 cm^{-1} (out of plane bending of outer C—H moiety), 701 cm^{-1} (C—N) and 661 cm^{-1}, that indicated the presence of **1** in the nanocomposite **1**/rGO/**Pyr-Py** [35,36]. Similarly, FT-IR spectra of **2**/rGO/**Pyr-Py** composite also showed the characteristic peaks of **2** and **Pyr-Py** (Fig. 3**d**).

2.3. Electrocatalytic oxygen reduction

Herein, the electrochemically catalyzed oxygen reductions of **1**/rGO/**Pyr-Py** and **1**/rGO nanocomposites were firstly investigated in the acid media. As shown in Fig. 4, the cyclic voltammetry data of **1**/rGO/

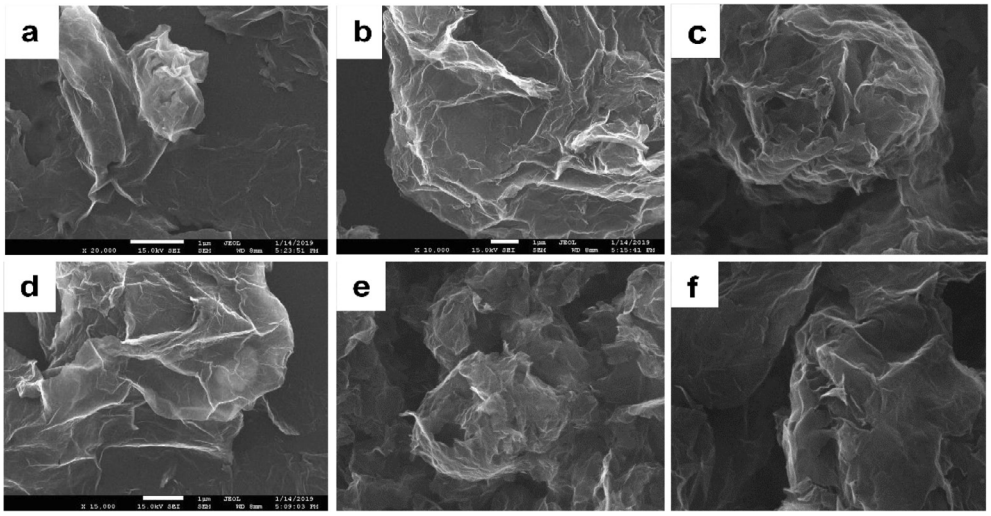

Fig. 2. SEM images of (a) rGO, (b) rGO/**Pyr-Py**, (c) **1**/rGO, (d) **1**/rGO/**Pyr-Py**, (e) **2**/rGO and (f) **2**/rGO/**Pyr-Py**.

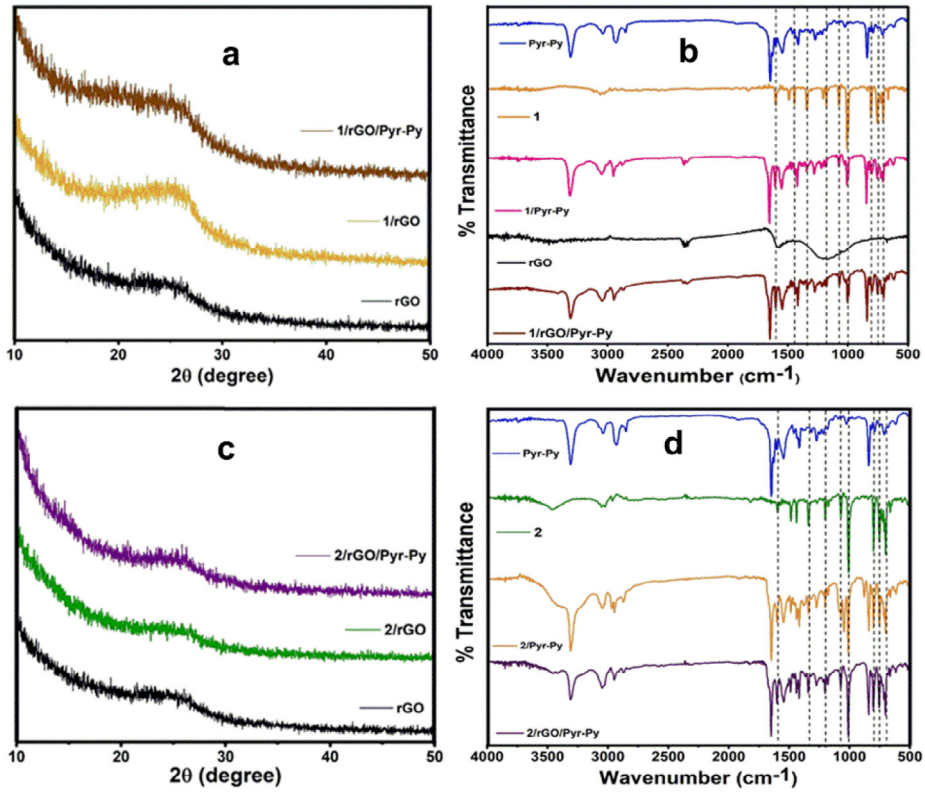

Fig. 3. (a) XRD patterns of rGO, **1**/rGO and **1**/rGO/**Pyr-Py**, (b) FT-IR spectra of **Pyr-Py**, **1** and **1**/rGO/**Pyr-Py** nanocomposites, (c) XRD patterns of **2**/rGO and **2**/rGO/**Pyr-Py**, and (d) FT-IR spectra of **Pyr-Py**, **2** and **2**/rGO/**Pyr-Py**.

Pyr-Py has a more positive onset potential and halve-wave potentials compared with that of **1**/rGO. Wei and co-workers reported the important role of a more positive onset and halve-wave potentials which is employed to evaluate the electrocatalytic activity of materials [14]. In addition, similar trends of enhanced electrochemically catalyzed behaviors were also observed in basic and neutral media where the onset potentials, halve-wave potentials and current densities of **1**/rGO/**Pyr-Py** are enhanced than **1**/rGO (Fig. 4**c–f**) owing to the presence of the axially coordinated **Pyr-Py**. The enhanced catalytic activity brought about by the **Pyr-Py** was further investigated using **2** as the catalyst to produce **2**/rGO/**Py-Py**.

In addition, when **2**/rGO/**Pyr-Py** and **2**/rGO were compared (Fig. 5), the positive effect brought up by our **Pyr-Py** ligand were also clearly confirmed. Liang *et al.,* tested the state-of-the-art Pt/C catalyst in KOH and reported a halve-wave value at 0.87 V (versus RHE) [37]. Cao et al., in KOH also found the halve wave potential of Pt/C at 0.88 V [38] which is consistent with Liang's work. These results compared to our material (**2**/rGO/**Pyr-Py**) showed a better electrocatalytic performance (0.90 V versus RHE, halve-wave potential) than state-of-the-art Pt/C in same media under our experimental condition. The summary of CV data of **1** and **2** with and without **Pyr-Py** on rGO towards ORR in all media is presented in Table 1. It is important to state that the reversible redox wave displayed at $E_{1/2}$ = 0.65 and 0.43 *vs* RHE is attributed to the iron porphyrins reversible Fe^{III}/Fe^{II} couple which is responsible for the electrocatalysis. On the other hand, a plot of current *vs* scan rates (10–500 mV s^{-1}) for **1**/rGO/**Pyr-Py**, **1**/rGO, **2**/rGO/**Pyr-Py** and **2**/rGO

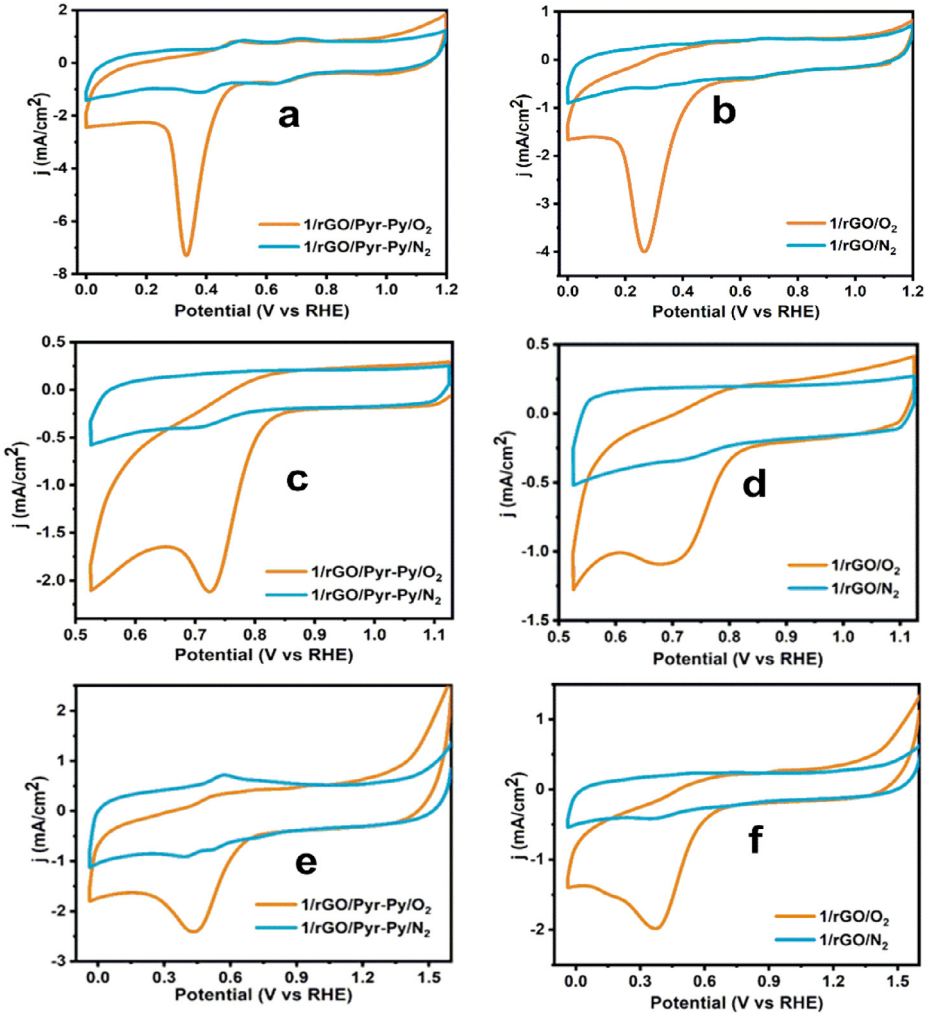

Fig. 4. CVs of GC electrodes coated with **1**/rGO/**Pyr-Py** and **1**/rGO in 0.5 M H_2SO_4 (a and b), 1.0 M KOH (c and d) and 0.1 M PBS (e-f) aqueous solutions under N_2 and O_2. Conditions: 50 mV s^{-1} scan rate at 25 °C.

in 0.1 M KOH were examined (Fig. S2, see ESI). A linear relationship between peak current and scan rate indicates the immobilized species are present. On the other hand, redox events of the catalyst materials appeared more clearer as scan rates increased illustrating more active sites are exposed. This further indicates the transition from Fe^{+3}/Fe^{+2} and Mn^{3+}/Mn^{2+} increases with increasing scan rates thereby exposing more active sites for catalysis.

On the other hand, kinetic activities derived from LSV for our materials in KOH are presented in Fig. 6. The Tafel slopes indicate higher kinetic rates with respect to **Pyr-Py** composites in the order **1**/rGO (116 mV/dec) < **1**/rGO/**Pyr-Py** (93 mV/dec) and **2**/rGO (110 mV/dec) < **2**/rGO/**Pyr-Py** (93 mV/dec) as shown in Fig. 6**a′** and **b′** respectively. The low Tafel slopes shown by our two target materials further elaborates the effectiveness of these materials to catalyze oxygen reduction reactions.

Electrochemical tests were performed using our target materials (**1**/rGO/**Pyr-Py** and **2**/rGO/**Pyr-Py**) in both acidic and basic environment to stability. Linear sweep voltammetry responses before and after 300 cycles revealed our target materials (metalloporphyrin/rGO/**Pyr-Py**) showing some levels of catalytic fading in both media (Fig. 7**a–d**). This fading especially in acidic medium, could be linked to protonation of aromatic nitrogen in pyridine that makes the complexation reaction a little unfavorable for longer cycles. Notably, the stability test showed **1**/rGO/**Pyr-Py** materials better than **2**/rGO/**Pyr-Py** (Fig. 7**a–d**). The superior stability exhibited by **1**/rGO/Pyr-Py illustrates a stronger coordination property between iron porphyrin and **Pyr-Py** moiety compared to that of manganese porphyrin. This property gives a more advantage of **1**/rGO/**Pyr-Py** over **2**/rGO/**Pyr-Py**.

2.4. Oxygen evolution reaction

Electrocatalytic OER properties of our composite materials were examined in 1.0 M KOH and LSV data shown in Fig. 8**a** and **b**. From the data, materials with **Pyr-Py** exhibited enhanced current density compared to the materials directly on rGO suggesting surpassing kinetics of these materials (metalloporphyrins/rGO/**Pyr-Py**). At j = 1.0 mA/cm^2 (1.481 V), **1**/rGO/**Pyr-Py** displayed an overpotential of 251 mV while **1**/rGO at the same current density recorded overpotential of 335 mV exhibiting a difference of 84 mV. Lower overpotential exhibited by **1**/rGO/**Pyr-Py** indicates its ability to evolve oxygen more than **1**/rGO. Also, at j = 10 mA/cm^2, **1**/rGO/**Pyr-Py** showed the lowest overpotential (521 mV) which is 109 mV lower than **1**/rGO whose overpotential was 630 mV. The OER activities of **2**/rGO/**Pyr-Py** and **2**/rGO were also monitored at j = 1.0 and 10 mA/cm^2 and the results reported in Table 2. In all aspects **2**/rGO/**Pyr-Py** showed lower overpotential compared to **2**/rGO as expected. This is another avenue to praise the catalytic enhancement effect of our **Pyr-Py** linker. To gain insight into kinetics of electrode reaction, we performed Tafel analysis using our LSV measurement (Fig. 8**a′** and **b′**). The analysis revealed a slope in the order **1**/rGO/**Pyr-Py** < **1**/rGO < rGO/**Pyr-Py** < rGO and **2**/rGO/**Pyr-Py** < **2**/rGO < rGO/**Pyr-Py** < rGO similar to that of ORRs. Marianov and co-workers in their experiment indicated a positive Tafel

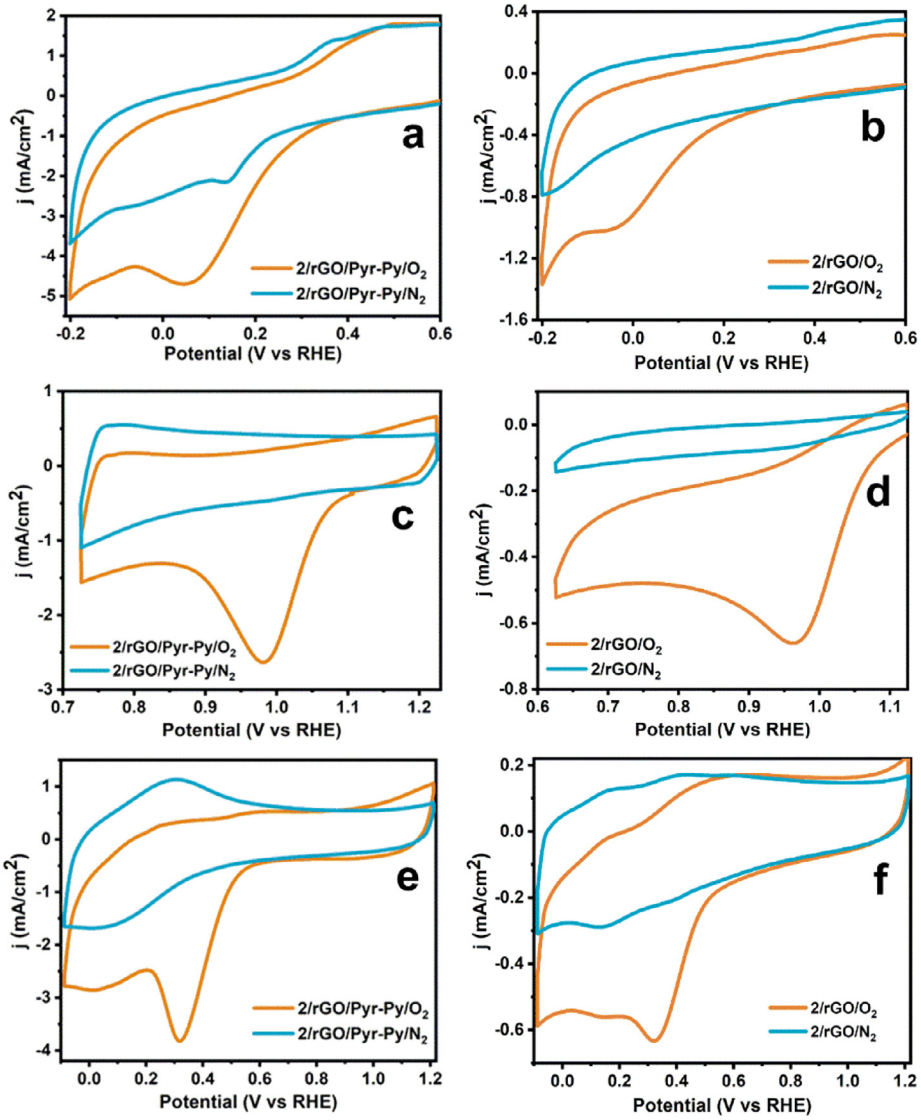

Fig. 5. CVs of GC electrodes coated with **2**/rGO/**Pyr-Py** and **2**/rGO in 0.5 M H_2SO_4 (a and b), 1.0 M KOH (c and d) and 0.1 M PBS (e-f) aqueous solutions under N_2 and O_2. Conditions: 50 mV s^{-1} scan rate at 25 °C.

Table 1
Comparison between ORR activities of composite materials in aqueous media.

Composite materials	Aqueous media	Onset-potential (V *vs* RHE)	Half-wave potential (V *vs* RHE)	Current density (mA/cm^2)
1/rGO/**Pyr-Py**	H_2SO_4	+0.535	+0.401	−7.314
	KOH	+0.859	+0.779	−2.127
	PBS	+0.689	+0.574	−2.431
1/rGO	H_2SO_4	+0.528	+0.352	−4.021
	KOH	+0.837	+0.740	−1.089
	PBS	+0.659	+0.506	−1.978
2/rGO/**Pyr-Py**	H_2SO_4	+0.345	+0.202	−4.699
	KOH	+1.101	+1.001	−2.368
	PBS	+0.579	+0.453	−3.808
2/rGO	H_2SO_4	+0.273	+0.100	−1.003
	KOH	+1.082	+0.991	−0.663
	PBS	+0.556	+0.430	−0.637

slope of above 230 mV/dec with their noncovalent immobilized MnTPP via carbon cloth [28]. Comparison of our Tafel slope for both **1**/rGO/**Pyr-Py** and **2**/rGO/**Pyr-Py** (216 mV/dec) to their work indicates a better kinetics of our material than their work. We have therefore once again demonstrated the enhanced electrocatalytic performance of our target materials towards catalysis.

3. Conclusion

In this work, a pyrene-pyridine hybrid (**Pyr-Py**) was employed as an axial ligand to bridge Fe(III)Cl-TPP and Mn(III)Cl-TPP through non-covalent immobilization on rGO. Comparatively, significantly enhanced electrocatalytic performance towards ORR and OER through axial ligand exchanging strategy was exhibited. Therefore, we are hopeful this strategy of integrating molecular catalysts on **Pry-Py** through axial ligation via rGO could enhance new applications in electrocatalysis towards ORR and OER.

Declaration of Competing Interest

The authors declare that they have no known competing financial interests or personal relationships that could have appeared to influence the work reported in this paper.

Acknowledgements

This work was financially supported by the National Natural Science

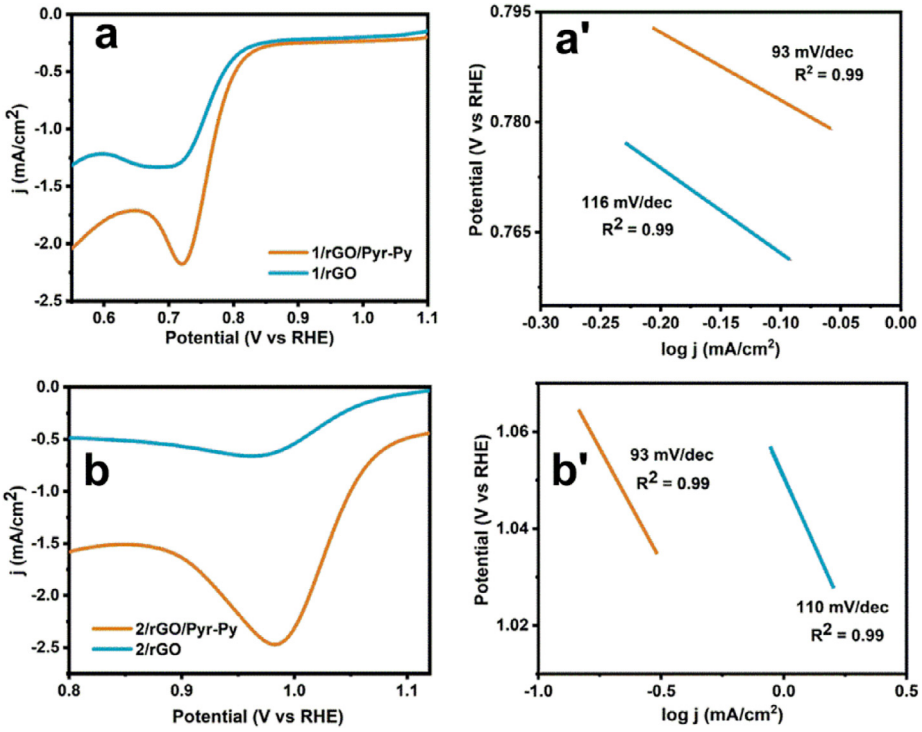

Fig. 6. LSV curves for **1**/rGO/**Pyr-Py**, **1**/rGO (a) and **2**/rGO/**Pyr-Py**, **2**/rGO (b) at 50 mV/s in 1.0 M KOH O_2 saturated solution at 25 °C with their corresponding Tafel Plots (a′ and b′).

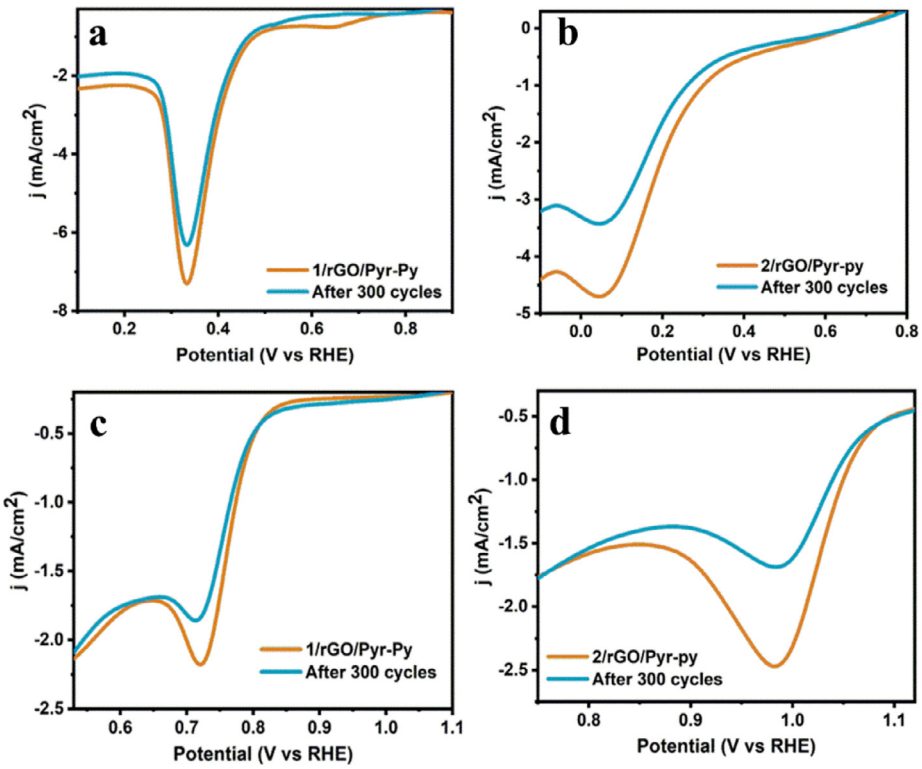

Fig. 7. LSV of GC coated with **1**/rGO/**Pyr-Py** (a) and **2**/rGO/**Pyr-Py** (b) before and after 300 cycles in 0.5 M H_2SO_4 (a and b) and 1.0 M KOH (c and d) at 50 mV s^{-1} scan rates.

Foundation of China (21701058), the Natural Science Foundation of Jiangsu province (BK20160499), the State Key Laboratory of Coordination Chemistry (SKLCC1817), the Key Laboratory of Functional Inorganic Material Chemistry (Heilongjiang University) of Ministry of Education, the China post-doc foundation (2018 M642183), the Lanzhou High Talent Innovation and Entrepreneurship Project (2018-RC-105) and the Jiangsu University (17JDG035).

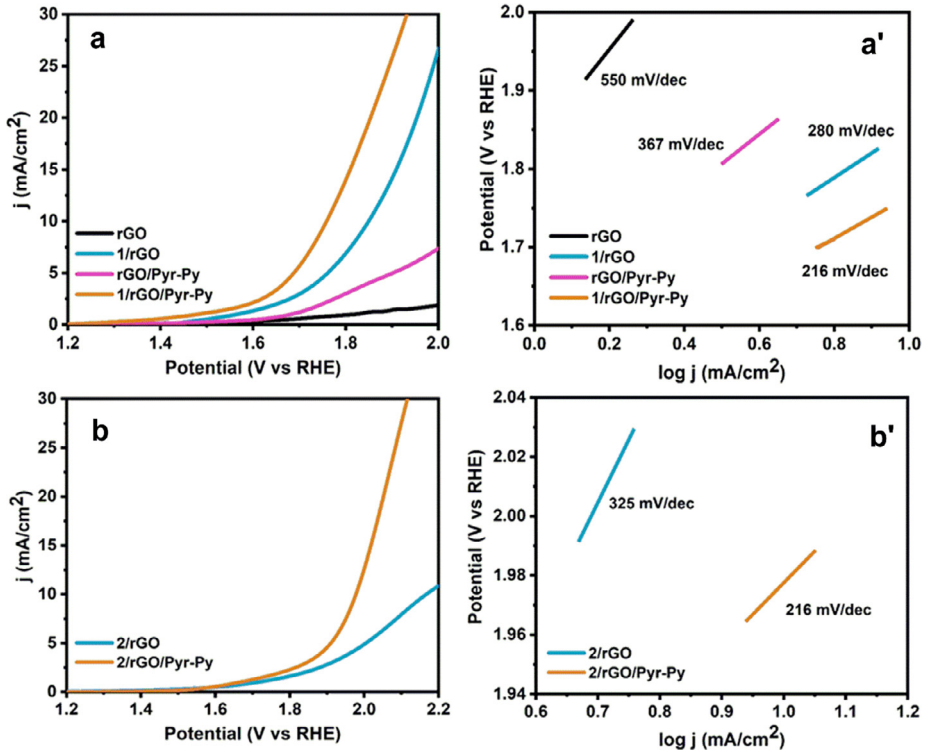

Fig. 8. LSV curves for **1**/rGO/**Pyr-Py**, **1**/rGO (a) and **2**/rGO/**Pyr-Py**, **2**/rGO (b) at 50 mV/s in 1.0 M KOH O_2 saturated solution at 25 °C with their corresponding Tafel Plots (a′ and b′).

Table 2
Comparison between OER activities of composite materials of **1** and **2** in KOH.

Composite materials	@ j = 1.0 (E/V)	Overpotential/ mV	@ j = 10 (E/V)	Overpotential/mV	Tafel slope/mV dec^{-1}
1/rGO/Pyr-Py	1.481	251	1.751	521	216
1/rGO	1.565	335	1.860	630	280
2/rGO/Pyr-Py	1.665	435	1.978	748	216
2/rGO	1.712	482	2.165	935	325

The OER overpotentials were calculated using the formula **overpotential (η) = E_{RHE} − 1.23 V**.

Author contributions

Mr. Isaac Kwaku Attatsi was responsible for experimental parts. The whole work was supervised and manuscript edited by Prof. Dr. Xu Liang and Prof. Dr. Weihua Zhu. The manuscript was well discussed by all authors.

Appendix A. Supplementary data

Supplementary data to this article can be found online at https://doi.org/10.1016/j.ica.2020.119584.

References

[1] Y. Kuang, Y. Zhang, B. Zhou, C. Li, Y. Cao, L. Li, L. Zeng, Renew. Sustain. Energy Rev. 59 (2016) 504–513.
[2] M.T. Gencoglu, Z. Ural, Int. J. Hydrog. Energy 34 (2009) 5242–5248.
[3] Y. Nie, L. Li, Z. Wei, Chem. Soc. Rev. 44 (2015) 2168–2201.
[4] Y. Xue, H. Chen, J. Qu, L. Dai, 2D Mater. 2 (2015) 044001.
[5] E.G. Kovaleva, J.D. Lipscomb, Nat. Chem. Biol. 4 (2008) 186.
[6] J. Hohenberger, K. Ray, K. Meyer, Nat. Commun. 3 (2012) 720.
[7] M.K. Debe, Nature 486 (2012) 43.
[8] Y.-C. Wei, C.-W. Liu, K.-W. Wang, Chem. Commun. 47 (2011) 11927–11929.
[9] J.-M. You, H.S. Han, H.K. Lee, S. Cho, S. Jeon, Int. J. Hydrog. Energy 39 (2014) 4803–4811.
[10] Z. Weng, J. Jiang, Y. Wu, Z. Wu, X. Guo, K.L. Materna, W. Liu, V.S. Batista, G.W. Brudvig, H. Wang, J. Am. Chem. Soc. 138 (2016) 8076–8079.
[11] P.K. Sonkar, K. Prakash, M. Yadav, V. Ganesan, M. Sankar, R. Gupta, D.K. Yadav, J. Mater. Chem. A 5 (2017) 6263–6276.
[12] P.K. Sonkar, V. Ganesan, R. Gupta, D.K. Yadav, M. Yadav, J. Electroanal. Chem. 826 (2018) 1–9.
[13] N.G. Sahoo, Y. Pan, L. Li, S.H. Chan, Adv. Mater. 24 (2012) 4203–4210.
[14] P.-J. Wei, G.-Q. Yu, Y. Naruta, J.-G. Liu, Angew. Chem. Int. Ed. 53 (2014) 6659–6663.
[15] L. Xiong, A. Manthiram, Electrochim. Acta 49 (2004) 4163–4170.
[16] Z. Zhang, H. Li, Y. Yang, J. Key, S. Ji, Y. Ma, H. Wang, R. Wang, RSC Adv. 5 (2015) 27112–27119.
[17] Y. Gorlin, B. Lassalle-Kaiser, J.D. Benck, S. Gul, S.M. Webb, V.K. Yachandra, J. Yano, T.F. Jaramillo, J. Am. Chem. Soc. 135 (2013) 8525–8534.
[18] J. Park, H. Kim, K. Jin, B.J. Lee, Y.-S. Park, H. Kim, I. Park, K.D. Yang, H.-Y. Jeong, J. Kim, J. Am. Chem. Soc. 136 (2014) 4201–4211.
[19] R. Bashyam, P. Zelenay, Materials for Sustainable Energy: A Collection of Peer-Reviewed Research and Review Articles from Nature Publishing Group, World Scientific, 2011, pp. 247–250.
[20] G. Wu, P. Zelenay, Acc. Chem. Res. 46 (2013) 1878–1889.
[21] S. Guo, S. Zhang, L. Wu, S. Sun, Angew. Chem. Int. Ed. 51 (2012) 11770–11773.
[22] M.J. Griffith, K. Sunahara, P. Wagner, K. Wagner, G.G. Wallace, D.L. Officer, A. Furube, R. Katoh, S. Mori, A.J. Mozer, Chem. Commun. 48 (2012) 4145–4162.
[23] M. Zhu, Y. Dong, Y. Du, Z. Mou, J. Liu, P. Yang, X. Wang, Chem. Eur. J. 18 (2012) 4367–4374.
[24] M. Zhu, Z. Li, B. Xiao, Y. Lu, Y. Du, P. Yang, X. Wang, ACS Appl. Mater. Interfaces 5 (2013) 1732–1740.
[25] M. Wang, Q. Wang, W. Zhu, Y. Yang, H. Zhou, F. Zhang, L. Zhou, J.M. Razal, G.G. Wallace, J. Chen, Green Energy Environ. 2 (2017) 285–293.
[26] G. Zuo, H. Yuan, J. Yang, R. Zuo, X. Lu, J. Mol. Catal. Chem. 269 (2007) 46–52.
[27] A. Marianov, Y. Jiang, ACS Sustain. Chem. Eng. 7 (2019) 3838–3848.
[28] J. Chlistunoff, J.-M. Sansinena, J. Phys. Chem. C 118 (2014) 19139–19149.
[29] Z. Wu, J. Appl. Polym. Sci. 110 (2008) 777–783.
[30] Y. Zhou, Y. Shi, F.-B. Wang, X.-H. Xia, Anal. Chem. 91 (2019) 2759–2767.
[31] R.Z. Snitkoff, N. Levy, I. Ozery, S. Ruthstein, L. Elbaz, Carbon 143 (2019) 223–229.
[32] H.-L. Guo, X.-F. Wang, Q.-Y. Qian, F.-B. Wang, X.-H. Xia, ACS Nano 3 (2009)

2653–2659.
[33] S. Liu, X. He, J. Zhu, L. Xu, J. Tong, Sci. Rep. 6 (2016) 35189.
[34] S. Liu, Z. Chen, N. Zhang, Z.-R. Tang, Y.-J. Xu, J. Phys. Chem. C 117 (2013) 8251–8261.
[35] D.R. Roy, E.V. Shah, S.M. Roy, Spectrochim. Acta A Mol. Biomol. Spectrosc. 190 (2018) 121–128.
[36] S. Paul, F. Amalraj, S. Radhakrishnan, Synth. Met. 159 (2009) 1019–1023.
[37] Y. Liang, Y. Li, H. Wang, J. Zhou, J. Wang, T. Regier, H. Dai, Nat. Mater. 10 (2011) 780.
[38] R. Cao, J. Lee, M. Liu, J. Cho, Adv. Energy Mater. 2 (2012) 816–829.